Supporting Information

Bowles *et al.* 10.1073/pnas.0806521105

SI Discussion

Structural Implications for an Oxidative Half-Reaction. After substrate oxidation and concomitant FAD reduction, dehydrogenases and oxidases must undergo an oxidative half-reaction to promote release of the substrate and regeneration of the starting enzyme (1). In the oxidases, electrons are transferred directly from the reduced FAD to molecular oxygen inside the active site (2), whereas the dehydrogenase active site flavin is inaccessible to molecular oxygen (3). As an alternative, dehydrogenases use electron-transferring flavoprotein (ETF) as the electron acceptor. The human ETF/MCAD cocrystal structure suggested that the interaction between ETF and a small hydrophobic pocket located on MCAD domain I (4) would allow the highly dynamic ETF FAD domain to sample available conformational space to position itself for rapid electron transfer with the *si*-face of flavin in the adjacent subunit. In contrast, domain IV at the C terminus of ACO blocks ETF to the *si*-face of flavin (2).

The similarity of AidB to both MCAD and ACO suggests that flavin oxidation by either ETF or molecular oxygen would be unlikely. On one hand, the solvent accessibility of the flavin ring and the pyrimidine moiety of AidB are similar to that of MCAD, likely preventing molecular oxygen from gaining access. On the other hand, the ETF binding site on domain I is only partially conserved in AidB. Moreover, the different dimer–dimer interface in AidB places subunit D in a position that would sterically occlude the ETF FAD domain, and the loops between $\beta1'$ and $\beta2'$ and between $\beta5$ and $\beta6$, as well the N-terminal extension, would block conformation sampling by the ETF FAD. If AidB were to employ FAD in a redox reaction, it appears that the oxidation half-reaction would have to occur in a manner distinct from that of MCAD or ACO. Alternatively, these observations raise the possibility that AidB does not use FAD as a redox cofactor.

SI Methods

Molecular Modeling. Docking of dsDNA onto AidB was performed by using HADDOCK 2.0 (5–7). A 12-bp segment of canonical B-DNA, generated with 3DNA (8), and one AidB dimer were used as starting structures. DNA binding residues Arg-468, Arg-469, Arg-475, and Lys-476, and Arg-518 and all DNA residues were used as active ambiguous interaction restraints (AIRs) with a distance limit of 3.0 Å. Residues 460–480, 515–522, and the DNA were allowed semiflexibility during simulated annealing, and C_2 symmetry was imposed on the dimer to enforce two-fold symmetry at the binding interface. Results of the solvent refinement were clustered with a 2.5-Å rmsd cutoff, and structures from the cluster with the best HADDOCK score were inspected manually.

Hydrodynamic Measurements. Gel filtration chromatographic analysis was performed on an analytical Superdex S-200 column (GE Healthcare) equilibrated in 50 mM Hepes (pH 6.8), 250 mM NaCl, 5% glycerol, 2 mM DTT, and 0.1 mM EDTA. A 50-μl solution of 1–2 mg/ml protein was eluted at 0.5 ml/min. Tetrameric AidB was observed at ionic strengths as high as 500 mM NaCl. The molecular mass standard curve was generated from a 50-μl solution containing thyroglobulin (670 kDa), aldolase (158 kDa), albumin (64 kDa), chicken ovalbumin (44 kDa), equine myoglobin (17 kDa), and vitamin B12 (1.4 kDa).

Sedimentation velocity analysis was conducted at 20°C and 40,000 rpm using interference optics with a Beckman–Coulter XL-I analytical ultracentrifuge. Four dilutions of AidB (0.09–1.15 mg/ml) were prepared in activity buffer. The data were initially analyzed by using the program DCDT+ (9), and the molecular weight and sedimentation coefficient ($S_{20,w} = 9.94$ S) were obtained by global fitting of the data sets collected at multiple concentrations to a hybrid discrete-continuous model with Sedphat (10).

1. Ghisla S, Thorpe C (2004) Acyl-CoA dehydrogenases. A mechanistic overview. *Eur J Biochem* 271:494–508.
2. Nakajima Y, *et al.* (2002) Three-dimensional structure of the flavoenzyme acyl-CoA oxidase-II from rat liver, the peroxisomal counterpart of mitochondrial acyl-CoA dehydrogenase. *J Biochem* 131:365–374.
3. Kim JJ, Miura R (2004) Acyl-CoA dehydrogenases and acyl-CoA oxidases. Structural basis for mechanistic similarities and differences. *Eur J Biochem* 271:483–493.
4. Toogood HS, *et al.* (2004) Extensive domain motion and electron transfer in the human electron transferring flavoprotein medium chain Acyl-CoA dehydrogenase complex. *J Biol Chem* 279:32904–32912.
5. Dominguez C, Boelens R, Bonvin AM (2003) HADDOCK: A protein-protein docking approach based on biochemical or biophysical information. *J Am Chem Soc* 125:1731–1737.
6. de Vries SJ, *et al.* (2007) HADDOCK versus HADDOCK: New features and performance of HADDOCK2.0 on the CAPRI targets. *Proteins* 69:726–733.
7. van Dijk M, van Dijk AD, Hsu V, Boelens R, Bonvin AM (2006) Information-driven protein-DNA docking using HADDOCK: It is a matter of flexibility. *Nucleic Acids Res* 34:3317–3325.
8. Lu XJ, Olson WK (2003) 3DNA: A software package for the analysis, rebuilding and visualization of three-dimensional nucleic acid structures. *Nucleic Acids Res* 31:5108–5121.
9. Philo JS (2000) A method for directly fitting the time derivative of sedimentation velocity data and an alternative algorithm for calculating sedimentation coefficient distribution functions. *Anal Biochem* 279:151–163.
10. Schuck P (2003) On the analysis of protein self-association by sedimentation velocity analytical ultracentrifugation. *Anal Biochem* 320:104–124.
11. Wallace AC, Laskowski RA, Thornton JM (1995) LIGPLOT: A program to generate schematic diagrams of protein-ligand interactions. *Protein Eng* 8:127–134.
12. Kim JJ, Wang M, Paschke R (1993) Crystal structures of medium-chain acyl-CoA dehydrogenase from pig liver mitochondria with and without substrate. *Proc Natl Acad Sci USA* 90:7523–7527.
13. Djordjevic S, Pace CP, Stankovich MT, Kim JJ (1995) Three-dimensional structure of butyryl-CoA dehydrogenase from Megasphaera elsdenii. *Biochemistry* 34:2163–2171.
14. Tiffany KA, *et al.* (1997) Structure of human isovaleryl-CoA dehydrogenase at 2.6 A resolution: Structural basis for substrate specificity. *Biochemistry* 36:8455–8464.
15. Pike, A. C. W., Hozjan, V., Smee, C., Berridge, G., Burgess, N., Salah, E., Bunkoczi, G., Uppenberg, J., Ugochukwu, E., Von Delft, F., Arrowsmith, C. H., Edwards, A., Weigelt, J., Sundstrom, M., and Oppermann, U. Crystal Structure of Human Very Long Chain Acyl-Coa Dehydrogenase (ACADVL), *PDB ID: 2UXW.*
16. Battaile KP, Nguyen TV, Vockley J, Kim JJ (2004) Structures of isobutyryl-CoA dehydrogenase and enzyme-product complex: Comparison with isovaleryl- and short-chain acyl-CoA dehydrogenases. *J Biol Chem* 279:16526–16534.
17. Nagpal A, Valley MP, Fitzpatrick PF, Orville AM (2006) Crystal structures of nitroalkane oxidase: Insights into the reaction mechanism from a covalent complex of the flavoenzyme trapped during turnover. *Biochemistry* 45:1138–1150.
18. Alfieri A, *et al.* (2007) Structure of the monooxygenase component of a two-component flavoprotein monooxygenase. *Proc Natl Acad Sci USA* 104:1177–1182.
19. Martins BM, Dobbek H, Cinkaya I, Buckel W, Messerschmidt A (2004) Crystal structure of 4-hydroxybutyryl-CoA dehydratase: Radical catalysis involving a [4Fe-4S] cluster and flavin. *Proc Natl Acad Sci USA* 101:15645–15649.
20. Battaile KP, *et al.* (2002) Crystal structure of rat short chain acyl-CoA dehydrogenase complexed with acetoacetyl-CoA: Comparison with other acyl-CoA dehydrogenases. *J Biol Chem* 277:12200–12207.

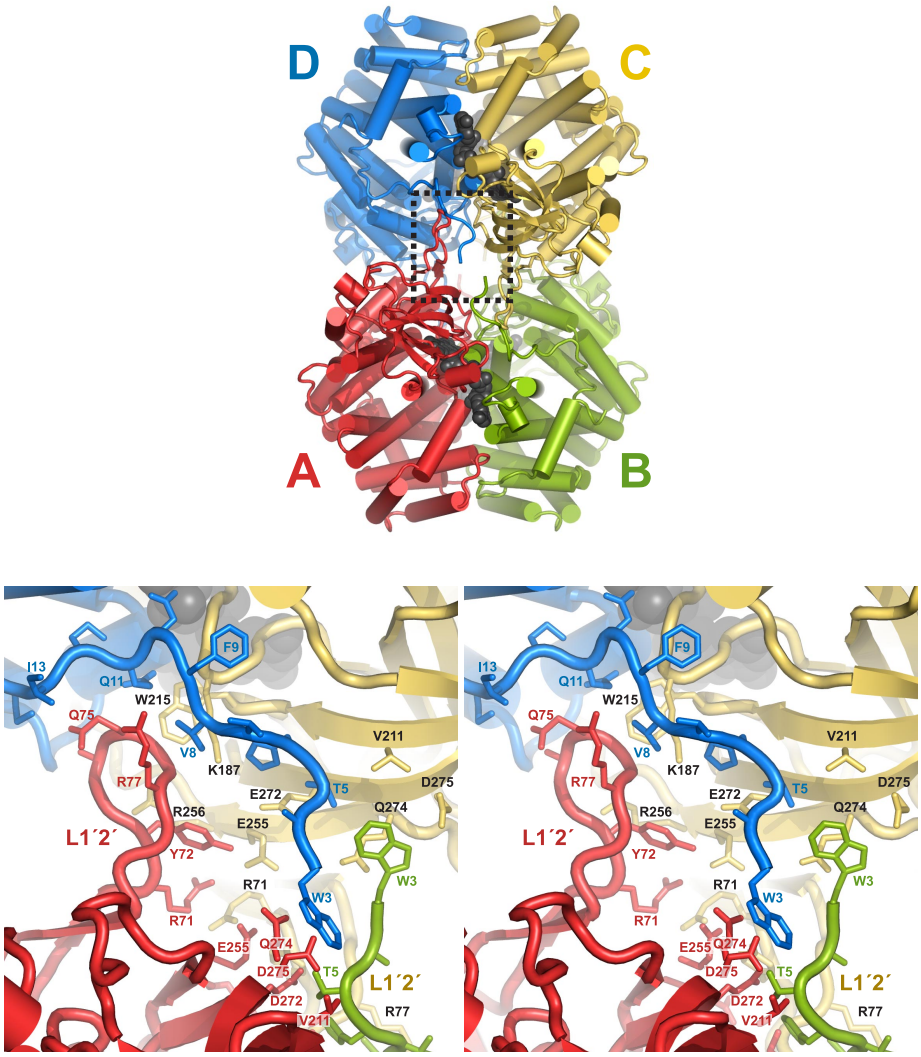

Fig. S1. Intersubunit contacts in the AidB tetramer. (*Upper*) Cartoon representation of the AidB tetramer colored by subunit A-D. FAD molecules are shown as black CPK spheres. The dashed boxed region is shown in detail in *Lower*. (*Lower*) Stereo view of the details of the tetramer interface, with subunits colored as in *Upper*. The L1′2′ loop from subunit A tucks into a pocket created by Val-8-Pro-14 on subunit D and Trp-215 on subunit C. Likewise, the N termini of subunits B and D associate with each other and with Gln-274-Asp-275 and Val-211 side chains from subunits C and A, respectively.

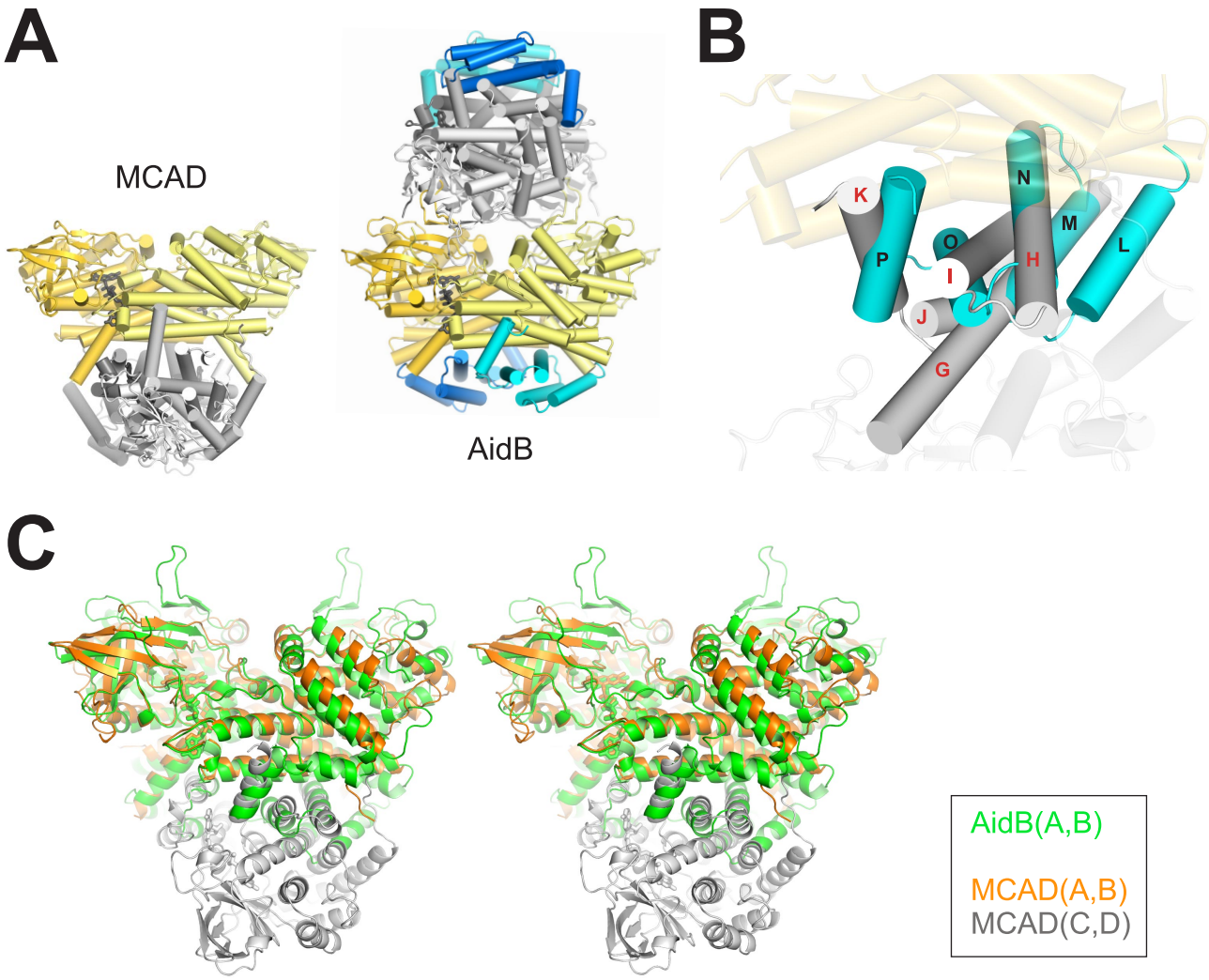

Fig. S2. The inverted AidB tetramer. (*A*) Cartoon representation of the MCAD and AidB tetramers. AB subunits are yellow/gold, and CD subunits are white/gray. AidB domain IV is colored blue (subunits A and C) and cyan (subunits B and D). (*B*) Superposition of AidB and ACAD AB dimers (transparent gold) places AidB domain IV (cyan) onto the MCAD CD dimer (silver). AidB helices αM, αN, αO, and αP correspond directly to MCAD helices αG, αH, αI/J, and αK (domain III). (*C*) Stereo view of the MCAD tetramer (AB, orange; CD, silver) superimposed on the AB dimer of AidB (green).

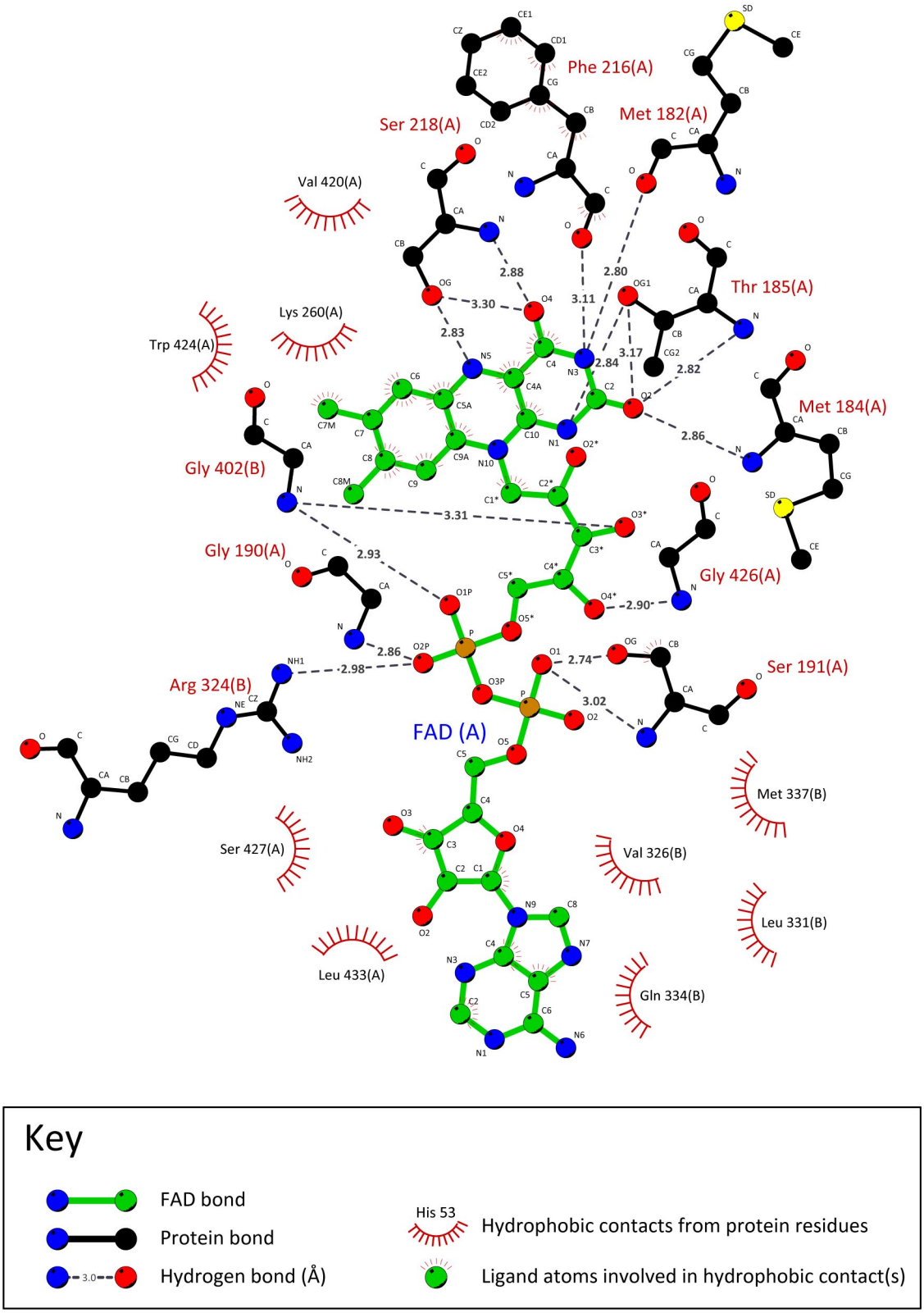

Fig. S3. Protein–FAD interactions. A schematic diagram generated by LIGPLOT (11) shows hydrogen bonding and hydrophobic interactions between FAD and AidB. FAD carbons are green, and protein carbons are black. Oxygen, red; phosphorus, orange; nitrogen, blue; sulfur, yellow. Letters in parentheses after residue numbers denote the protein subunit.

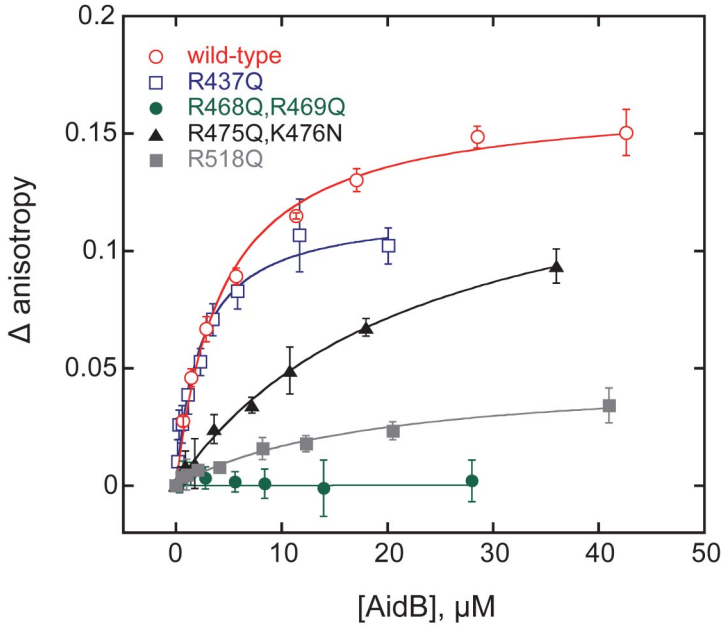

Fig. S4. DNA binding of AidB mutants. Fluorescence anisotropy binding isotherms for wild-type and mutant AidB proteins in complex with fluorescein-labeled dsDNA are shown. Error bars represent the standard deviation from the average of three independent experiments.

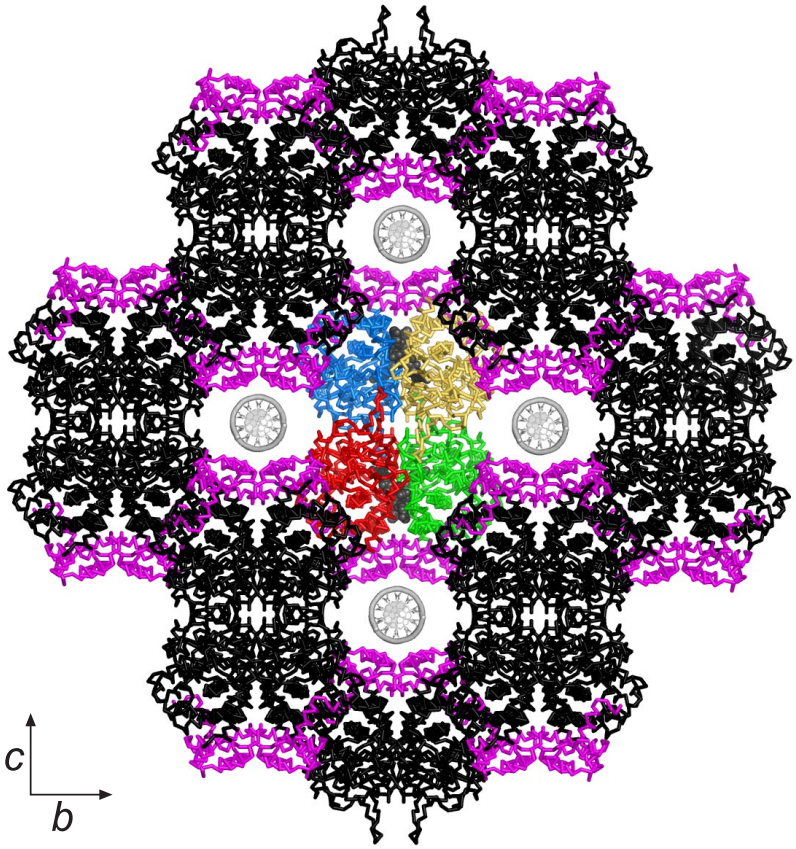

Fig. S5. AidB crystal packing. The I222 crystal form is shown, with the view down the crystallographic *a* axis. Proteins are shown as Cα backbone traces. For reference, one AidB tetramer is colored by subunit (red, green, gold, and blue) in the middle of the figure, with FADs as charcoal CPK spheres. Symmetry-related tetramers are colored black, and the C-terminal DNA binding domain is colored magenta throughout. DNA helices modeled into the 25-Å pores between DNA binding domains are shown on end as silver cartoons. In the I222 lattice (shown), one subunit (e.g., red) comprises the asymmetric unit, with the other three subunits in the tetramer related by crystallographic symmetry. The intermolecular packing is virtually identical in the $P3_1$ lattice (data not shown), except that one entire tetramer resides in the asymmetric unit.

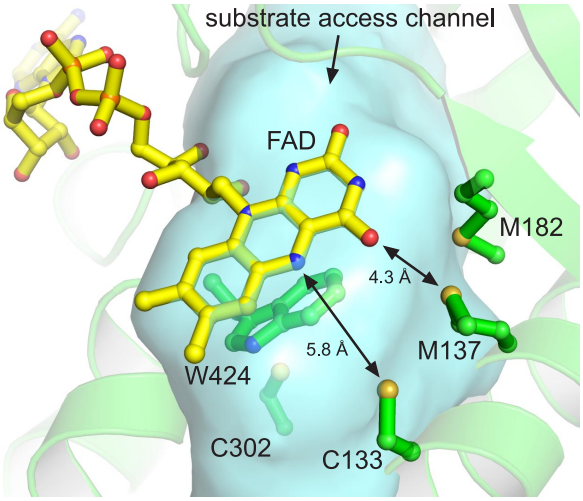

Fig. S6. The sulfur-rich FAD binding pocket of AidB. The solvent-accessible surface of the substrate access channel is shown in transparent blue and is lined with Cys-133, Met-137, Met-182, Cys-302, and the *re*-face of the FAD isoalloxazine ring (yellow carbons). Trp-424 is imbedded within this channel.

Table S1. Data collection, phasing, and refinement statistics for *E. coli* AidB

	Native	Hg	Se-1	Se-2
Cell parameters				
a, Å	85.0	84.8	84.7	139.9
b, Å	101.9	101.7	102.1	139.9
c, Å	137.6	137.9	137.1	126.3
α, °	90	90	90	90
β, °	90	90	90	90
γ, °	90	90	90	120
Space group	I222	I222	I222	$P3_1$
Proteins/asu	1	1	1	4
Data collection				
Wavelength, Å	1.02891	0.97746	0.97893	0.97869
Resolution, Å	50–1.7 (1.76–1.70)	50–2.5 (2.59–2.50)	50–1.92 (1.99–1.92)	50–3.0 (3.1–3.0)
Unique reflections	62,854 (4,844)	21,023 (2,070)	45,511 (4,488)	107,650 (10,493)
Completeness, %	95.7 (74.8)	100.0 (100.0)	100.0 (100.0)	97.2 (94.9)
Redundancy	12.6 (6.0)	16.4 (15.8)	12.4 (11.4)	14.0 (5.7)
R_{sym}*	0.053 (0.223)	0.086 (0.298)	0.101 (0.402)	0.079 (0.249)
$\langle I \rangle / \langle s(I) \rangle$	80.9 (8.8)	40.4 (10.5)	38.6 (5.6)	14.0 (5.7)
Phasing				
Resolution, Å		50–2.5	50–1.92	
No. of sites		16	21	
Phasing power (c/a)†		1.682/1.516	0.726/0.842	
Phasing power (anom)		1.069	1.691	
R_{cullis} (c/a)‡		0.608/0.865	1.009/0.967	
R_{cullis} (anom)		0.795	0.606	
Refinement				
Resolution	50–1.7 (1.8–1.7)			50–3.0 (3.2–3.0)
No. of reflections	59,648 (6,889)			25,801 (3,771)
R_{cryst}§	0.161 (0.182)			0.183 (0.244)
R_{free}§	0.179 (0.230)			0.228 (0.310)
No. of atoms				
Protein/FAD	4,225			16,672
Solvent	442			0
Average B factor, Å^2	20.3			37.4
rmsd bonds, Å	0.017			0.005
rmsd angles, °	1.616			0.906

Values in parentheses refer to data in the highest-resolution shell. c/a, centric/acentric data.

*$R_{sym} = \Sigma_{hkl}\Sigma_j I_j - \langle I \rangle / \Sigma_{hkl}\Sigma_j I_j$ where $\langle I \rangle$ is the mean intensity of *j* observations of reflection *hkl* and its symmetry equivalents.

†Phasing power $= \Sigma_{hkl} F_H / \Sigma_{hkl} |F_{PH} - F_{PH,calc}|$.

‡$R_{cullis} = (\Sigma_{hkl} ||F_{PH} \pm F_P| - F_{H,calc}|) / \Sigma_{hkl} |F_{PH} - F_P|$.

§$R_{cryst} = \Sigma_{hkl} |F_{obs} - kF_{calc}| / \Sigma_{hkl} |F_{obs}|$. $R_{free} = R_{cryst}$ for 5% of reflections that were not used in refinement.

Table S2. Structural homologs of *E. coli* AidB

PDB ID code	Abbreviation	Protein	Reference	rmsd, Å	DALI *Z*-score
3MDE	MCAD	Medium-chain acyl-CoA dehydrogenase	12	1.47	31.3
1BUC	bSCAD	Butyryl-CoA dehydrogenase	13	1.47	N/A
1IVH	IVD	Isovaleryl-CoA dehydrogenase	14	1.53	N/A
2UXW	ACADVL	Very-long-chain acyl-CoA dehydrogenase	15	1.58	N/A
1RXO	IBD	Isobutyryl-CoA dehydrogenase	16	1.59	N/A
2C0U	NAO	Nitroalkane oxidase	17	1.63	24.6
1IS2	ACO	Acyl-CoA oxidase II	2	1.65	20.6
2JBR	HPAH	*p*-Hydroxylphenylacetate hydroxylase	18	1.93	23
1U8V	HBD	4-Hydroxybutyryl-CoA dehydratase	19	2.36	15
1JQI	rSCAD	Short-chain acyl-CoA dehydrogenase	20	2.43	N/A

Proteins with structural similarity to *E. coli* AidB were identified by using the DALI server. Entries lacking a *Z*-score were identified from manual inspection of acyl-CoA dehydrogenases found in the primary literature and in the Protein Data Bank.